

1 Short title for running header: Permafrost mapping

2 **A new approach to mapping permafrost and change**
3 **incorporating uncertainties in ground conditions and**
4 **climate projections**

5
6 **Yu Zhang¹, Ian Olthof¹, Robert Fraser¹, and Stephen A. Wolfe²**

7 ¹ Canada Centre for Mapping and Earth Observation, Natural Resources Canada, Ottawa,
8 Ontario, K1A 0E4, Canada

9 ² Geological Survey of Canada, Natural Resources Canada, Ottawa, Ontario, K1A 0E8,
10 Canada

11 Correspondence to: Yu Zhang (yu.zhang@nrcan.gc.ca)

12
13 **Abstract**

14 Spatially detailed information on permafrost distribution and change with climate is important
15 for land-use planning, infrastructure development and environmental assessments. However,
16 the required soil and surficial geology maps in the North are coarse, and projected climate
17 scenarios vary widely. Considering these uncertainties, we propose a new approach to
18 mapping permafrost distribution and change by integrating remote sensing data, field
19 measurements, and a process-based model. Land-cover types from satellite imagery are used
20 to capture the general land conditions and to improve the resolution of existing permafrost
21 maps. For each land-cover type, field observations are used to estimate the probability of
22 different ground conditions. A process-based model is used to quantify the evolution of
23 permafrost for each ground condition under three representative climate scenarios (low,
24 medium and high warming). From the model results, the probability of permafrost occurrence
25 and the most likely permafrost conditions are determined. We apply this approach at 20 m
26 resolution to a large area in Northwest Territories, Canada. Mapped permafrost conditions are
27 in agreement with field observations and other studies. The data requirements, model
28 robustness and computation time are reasonable, and this approach may serve as a practical
29 means to mapping permafrost and changes at high resolution in other regions.

1 **1 Introduction**

2 About a quarter of the land in the northern hemisphere is underlain by permafrost (Zhang et
3 al., 1999). Climate in northern high latitudes has warmed at about twice the rate of the global
4 average during the 20th century, and continued warming is projected for the 21st century
5 (ACIA, 2005). Climate warming causes ground temperature increasing, active-layer
6 thickening, talik formation, and thawing of permafrost (Vaughan et al., 2013). These changes
7 have significant impacts on infrastructure foundations, hydrology, ecosystems, and feedbacks
8 to the climate system (ACIA, 2005). Mapping the distribution of permafrost and its possible
9 changes with climate is important for land-use planning, infrastructure development,
10 ecological and environmental assessments, and modelling the climate system.

11 Different approaches have been used to map permafrost. Due to lack of field data in the early
12 years, Wild (1882) delineated the southern boundary of permafrost in Russia using a model
13 and air temperature. Later on, more field data were included in drawing the boundary of
14 permafrost (see reviews by Nelson, 1989; Heginbottom, 2002; Shiklomanov, 2005). With
15 more field experience and observations available, permafrost distribution was divided into
16 continuous and discontinuous zones, and the latter was further divided into two to four sub-
17 zones (Heginbottom, 2002). Permafrost zones were defined based on spatial continuity, i.e.,
18 the proportion of an area underlain by permafrost (Heginbottom et al., 1995; Brown et al.,
19 1998). The most widely used permafrost maps are based on this concept, with boundaries
20 delineated using mean annual air temperature, field observations, and regional physiography
21 (Nikiforoff, 1928; Heginbottom et al., 1995; Brown et al., 1998). These maps are coarse in
22 spatial resolution (usually without an explicit spatial resolution) with broad categories;
23 therefore they have limited utility for practical land-use planning and engineering applications
24 or as a basis for assessing the impacts of climate change on permafrost.

25 Permafrost distribution can be mapped at high spatial resolution by aerial-photography
26 interpretation for some regions (Vitt et al. (1994; Reger and Solie, 2008). However, the
27 association between land surface features and permafrost conditions has to be clear and
28 interpretation needs good knowledge and experience. Several studies map permafrost
29 distribution by classifying satellite images (e.g., Morrissey et al., 1986; Leverington and
30 Duguay, 1997; Nguyen et al., 2009). These studies show the importance of ground conditions
31 (vegetation, soil and hydrological conditions) on permafrost distribution. Since permafrost
32 cannot presently be directly imaged by optical satellite-based sensors, permafrost condition

1 must be indirectly derived from permafrost related and remote-sensing detectable geophysical
2 or surface factors. However, the relation between these factors and permafrost conditions are
3 complex and may change with space and time (Leverington and Duguay, 1997; Duguay et al.,
4 2005).

5 Permafrost is a ground thermal condition rather than a substance. The impact of climate
6 change on permafrost distribution was recognized long-time ago (Wild, 1882), and now it is
7 an important issue for northern land-use planning, infrastructure development and global
8 climate projections (ACIA, 2005). Woo et al. (1992) estimated the shift in boundaries of
9 continuous and discontinuous permafrost in Canada by assuming a 4-5 °C increase in surface
10 temperature across the country. The Stefan solution, the frost-index method (Nelson and
11 Outcalt, 1983; 1987), Kudryavtsev's approach (Kudryavtsev et al. 1974), and the temperature at
12 the top of permafrost (TTOP) model (Smith and Riseborough, 1996) are some of the major
13 developments for mapping permafrost in recent years. These approaches integrate the effects
14 of air temperature, snow and ground conditions in simplified ways and can be used to map
15 permafrost spatially explicitly and to assess the effects of climate change (e.g., Anisimov and
16 Nelson, 1997; Wright et al. 2003). For mountain regions, Haeberli (1973) developed a method
17 to map permafrost using the Basal Temperature of Snow (BTS) in Alps and it has been used
18 in many high elevation areas. The method was further improved by including the effects of
19 topography on air temperature, solar radiation, and snow conditions, and by incorporating
20 field observations using permafrost probabilities for high resolution permafrost mapping (e.g.,
21 Lewkowicz and Ednie, 2004; Bonnaventure et al., 2012) and spatial sensitivity analysis to
22 climate change (Bonnaventure and Lewkowicz, 2013). Recently, Gruber (2012) developed a
23 global high-resolution (30 arc-second, or < 1 km) permafrost map using relations between air
24 temperature and probability of permafrost occurrence. Although these methods emphasized
25 the importance of climate on permafrost, they assume that permafrost is in equilibrium with
26 the atmospheric climate (therefore, they are categorized as equilibrium models by
27 Riseborough et al. (2008)). However, ground temperature observations show that current
28 permafrost conditions are not in equilibrium (Osterkamp, 2005), and modelling studies show
29 that the response of permafrost to climate warming during the 21st century will be transient
30 and non-equilibrium (Zhang et al., 2008; Zhang, 2013). In addition, these methods use simple
31 parameterization and statistic representation to consider the effects of ground conditions on
32 permafrost (e.g., the seasonal n-factor). They tend to under-estimate the complexity and

1 importance of ground conditions on permafrost dynamics, and the empirical parameters may
2 change with time and space.

3 In the past two decades, process-based models have been used to quantify the impacts of
4 climate change on permafrost conditions and their spatial distributions. Process-based models
5 can integrate climate and ground variables and capture transient processes from seasonal to
6 long-term changes, but they require detailed input data and computation time. Most spatial
7 modelling studies, especially at national to global scales, have been conducted at half-degree
8 latitude/longitude or coarser spatial resolutions (e.g., Lawrence and Slater, 2005; Marchenko
9 et al., 2008; Zhang et al., 2008). At such resolutions, it is difficult to consider detailed spatial
10 variations in vegetation and ground conditions, and the results are not suitable for land-use
11 planning and engineering applications. Recently, several studies have modelled and mapped
12 permafrost at finer spatial resolutions (Duchesne et al., 2008; Jafarov et al., 2012; Zhang et
13 al., 2012; 2013). In the North, however, the required maps for soil and ground conditions are
14 coarse, with polygons in soil and surficial geology maps usually covering more than a
15 hundred square kilometres. The lack of detailed soil and ground information is a major source
16 of uncertainty for high resolution permafrost mapping (Zhang et al., 2012; 2013). Another
17 source of uncertainty is climate change projections. Projected permafrost conditions differ
18 significantly under different climate scenarios (Anisimov and Reneva, 2006; Zhang et al.,
19 2008; 2012, 2013; Zhang, 2013), and consequently such results are difficult for decision
20 makers to use.

21 In this study, we develop a new approach to mapping permafrost and change in a more
22 objective, replicable and quantitative way and incorporating uncertainties in ground
23 conditions and climate projections. This approach integrates remote sensing, field
24 observations, and modelling in a practical way to map permafrost at high spatial resolution.
25 The mapped permafrost probability is similar to the concept of the traditional permafrost
26 zones. In the paper, we describe the methodology of the approach and demonstrate its
27 application for a large area in northern Canada.

2 Methodology

2.1 Approach and methods

2.1.1 A general description of the approach

Figure 1 shows the scheme of the new permafrost mapping approach. A land-cover map from satellite images is used to represent the general land conditions and to improve the spatial resolution of the final products. For each land-cover type, the probability of different ground conditions is estimated based on field observations. The evolution of permafrost was simulated using a process-based model for each ground-type under three representative climate change scenarios (low, medium and high warming). From these model outputs, the probability of permafrost occurrence and the most likely permafrost conditions are determined for each land-cover type. The following is the rationale and feasibility of the approach.

Climate, especially air temperature, is the dominant factor controlling the spatial distribution of permafrost at large scales (from a hundred kilometres to continental scales). However, in a small area within which the climate is somewhat similar, permafrost can be present or absent, and if present, the permafrost conditions can be significantly different from place to place (Shur and Jorgenson, 2007). Such local variation depends primarily on the distribution of vegetation and ground conditions, including soil composition, snow, topography, and drainage (e.g., Brown, 1973; Shur and Jorgenson, 2007; Morse et al., 2012). High resolution land-cover maps developed from satellite imagery can capture some general features of soil and hydrological conditions, which can explain some of the major differences in permafrost conditions (Nelson et al., 1997; Nguyen et al., 2009; Jorgenson et al., 2010). However, satellite images, especially optical images, only contain information about vegetation and near surface conditions. Therefore ground conditions within a land-cover type developed by satellite images can vary substantially. For example, hollows and hummocks are common at local scales, and there are also topographically controlled variations at large scales. Such differences can cause significant variations in permafrost conditions (Duguay et al., 2005; Zhang et al., 2013). Field observations show that organic layer thickness (OLT) on the top of the mineral soil, including mosses and lichens, is a dominant factor affecting active-layer thickness and ground temperature (e.g., Harris, 1987; Kasischke and Johnstone, 2005; Johnson et al., 2013). Model sensitivity tests also indicate that OLT is the most sensitive

1 factor affecting active-layer thickness and ground thermal conditions (Yi et al., 2007; Zhang
2 et al., 2012; Riseborough et al., 2013). Therefore, we used OLT to divide soil conditions into
3 several ground-types within a land-cover type. As current remote sensing technologies have
4 difficulties measuring OLT, we estimated the probability distribution of OLT based on field
5 observations for each land-cover type. Other input parameters for ground conditions,
6 including mineral soil texture, organic matter content in mineral soils, gravel fractions,
7 drainage parameters, and snow-drifting parameters, can be estimated based on land-cover
8 features, field observations, and soil and surficial geology maps. These parameters may be
9 unique for each ground-type or the same for all ground-types within a land-cover type. Land-
10 cover maps can be developed from satellite remote sensing images. Leaf area indices (LAI)
11 and wild fire history can also be estimated using optical satellite images.

12 Higher spatial resolution monthly climate data, necessary for spatial modelling, have been
13 developed by interpolating station observations (Wang et al., 2006; McKenney et al., 2011).
14 The temporal patterns of air temperature and precipitation can be estimated using
15 observations at climate stations (Zhang et al., 2012; 2013) or from re-analysis of climate
16 observations. Water vapour pressure can be estimated based on daily minimum air
17 temperature, and daily total insolation without topographic effects can be estimated using
18 latitude, the day of the year, the diurnal temperature range (Zhang et al., 2012). Topographical
19 effects on solar radiation can be calculated using a digital elevation model (Zhang et al.,
20 2013). To consider the uncertainty of future climate projections, three scenarios (low, medium
21 and high warming) can be selected to represent the medium and general range of the probable
22 scenarios based on climate model projections. If we assume that the low and high warming
23 scenarios represent the lower and upper quartiles of the probable scenarios and the medium
24 warming scenario represents the two middle quartiles, the probabilities of the low, medium
25 and high warming scenarios would be 0.25, 0.5, and 0.25, respectively.

26 To map permafrost and its evolution, permafrost dynamics for each grid cell are modelled
27 under the possible ground-types and the three representative climate scenarios. The
28 probability of permafrost occurrence in a grid cell can be determined based on the
29 probabilities of the ground-types and climate scenarios. In turn, the distributions of permafrost
30 probability and the most likely permafrost conditions can be mapped. The probability of
31 permafrost within a grid cell can be interpreted as a probability due to the uncertainties in

ground conditions and climate projections, or can be interpreted as permafrost proportion or extent due to spatial heterogeneity within the grid cell, especially when the grid cell is large.

2.1.2 Estimating the probability of ground-types within each land-cover type

The probability distribution of ground-types in all the areas of a land-cover type was estimated using a modified logistic function based on field sampling observations of OLT at different locations. We did the modification because OLT cannot be negative and is usually thicker than a certain value for peatlands and some other northern land types.

$$F(x) = (1 - e_{x0}/e_x) / (1 + e_x) \quad (x \geq x_0), \quad (1)$$

where

$$e_x = \exp[-(x - \mu)/s], \quad (2)$$

$$e_{x0} = \exp[-(x_0 - \mu)/s]. \quad (3)$$

Where x is OLT (cm) and $F(x)$ is the cumulative distribution probability of OLT for a land-cover type. x_0 is the minimum OLT (cm) of the land-cover type, μ and s (in centimetres) are the average and the standard deviation of the logistic distribution. The probability density can be derived as,

$$f(x) = \frac{e_x(1 + e_{x0})}{s \cdot e_{x0}(1 + e_x)^2} \quad (x \geq x_0), \quad (4)$$

where $f(x)$ is the probability density function. The probability of a ground-type i can be determined using Equation (4)

$$p(i) = \int_{a_i}^{b_i} f(x) dx = (1 + 1/e_{x0}) [1/(1 + e_{bi}) - 1/(1 + e_{ai})], \quad (5)$$

where $p(i)$ is the probability of a ground-type i for OLT ranging from a_i to b_i . The values of e_{ai} and e_{bi} are calculated from Equation (2) when x equals a_i and b_i , respectively. The value of i ranges from 1 to N , where N is the number of ground-types. The thinnest and thickest OLT ground-types can be determined from Equation (5) using a predetermined probability level (e.g., 0.1). Then, the OLT ranges of the other ground-types can be defined. The three parameters in Equation (1) (x_0 , μ and s) can be determined by comparing the fitted cumulative probability with the observed relative cumulative frequency. Figure 2 shows an example of distribution of ground-types in a land-cover type. For the model input, the OLT of a ground-

type was represented by $0.5(a_i+b_i)$, except for the thinnest and thickest OLT ground-types, which were determined as the OLT at which the cumulative probability $F(x)$ equals a predetermined probability level (0.05 and 0.95 for the thinnest and thickest OLT ground-types, respectively).

Sensitivity tests showed that the modelled average permafrost conditions converged quickly with the increase in the number of ground-types. Permafrost conditions were similar when the difference of the OLT was less than 5 cm, especially when OLT was thicker than 30 cm. Permafrost conditions were not sensitive to the changes in OLT when OLT was thicker than 50 cm (Zhang et al., 2012; Riseborough et al., 2013). Based on this response we can select the thickness and the number of ground-types.

2.1.3 The model

The permafrost condition and its changes with climate for each ground-type were quantified using the Northern Ecosystem Soil Temperature model (NEST). NEST is a one-dimensional transient model that considers the effects of climate, vegetation, snow, and soil conditions on ground thermal dynamics based on energy and mass transfer through the soil-vegetation-atmosphere system (Zhang et al., 2003). Ground temperature is calculated by solving the one-dimensional heat conduction equation. The dynamics of snow depth, snow density and their effects on ground temperature are considered. Soil water dynamics are simulated considering water input (rainfall and snowmelt), output (evaporation and transpiration), and distribution among soil layers. Soil thawing and freezing, and associated changes in fractions of ice and liquid water, are determined based on energy conservation. Detailed description of the model and validations can be found in Zhang et al. (2003; 2005; 2006). Lateral flows and snow drifting are parameterized in a simplified way (Zhang et al., 2002; 2012). The model can also consider the effects of topography on solar radiation (Zhang et al., 2013).

2.2 Applying the approach to an area in northern Canada

2.2.1 Study area and field observations

We applied this approach to a 94 km by 94 km area in Northwest Territories, Canada, centred at 62.77° N, 114.27° W (Fig. 3a). The area is located in the Great Slave Geological Province, a region of high mineral resource development in northern Canada, where seasonal and all-weather roads and other infrastructure are important. With the effects of the last glacial ice

1 sheet and the glacial lake McConnell, most of the surficial geology consists of fine-grained
2 glaciolacustrine sediments and wave-washed bedrock (Wolfe et al., 2013). The study area
3 includes the Great Slave Lowlands and Uplands with vegetation ranging from dense forest to
4 arctic tundra (Ecological Classification Group, 2007). The Great Slave Lowlands are poorly-
5 drained low relief terrain characterized by numerous water bodies separated by fens,
6 peatlands, mixed woodlands, white birch (*Betula papyrifera*) and black spruce (*Picea*
7 *mariana*) forests, whereas the Uplands are areas of higher relief and bedrock outcrops.
8 Permafrost in the region is discontinuous and highly variable, usually with abrupt transitions
9 from frozen to unfrozen ground over short distances (Wolfe et al., 2011). Therefore it is
10 important to provide spatially detailed information about permafrost conditions and possible
11 changes with climate warming. We selected this area also because it covers a large spatial
12 environmental and vegetation gradient and many field observations are available. In this area,
13 the thirty-year (1971-2000) mean annual air temperature ranged from -6.9 °C to -4.9 °C (Fig.
14 3f), and mean annual total precipitation ranged from 288 mm to 309 mm. Monthly mean air
15 temperature varied from -29 °C in January to 16 °C in July.

16 We conducted fieldwork in this area in 2005 and 2011. Data were collected on land-cover
17 types, vegetation conditions, surface OLT, and soil profile conditions (depths of the horizons,
18 texture and organic matter content), drainage, and summer thaw depths. We also collected
19 observations made by other investigators in this area (Gaanderse, 2011; Brown, 1973;
20 Karunaratne et al., 2008; Roujanski et al., 2012). In total, we compiled 124 observation sites
21 (Fig. 3b). Most sites were located near roads in the south providing easy access. Wolfe et al.
22 (2014) also identified 1777 lithalsas in the Great Slave Lowlands and Uplands using 1:60000
23 scale aerial photos acquired between 1978 and 1980, in which 955 sites were within our study
24 area (Fig. 3b). Lithalsas are permafrost mounds formed by ice segregation within mineral soil.
25 These field data and lithalsa observations were used to validate the modelled permafrost
26 distribution.

27 2.2.2 Land-cover types and the probability of ground-types

28 The land-cover types (Fig. 3c) were classified using SPOT High-Resolution Visible and
29 Infrared images. The area is covered by a SPOT 4 image acquired on 7 August 2008 and a
30 SPOT 5 image from 4 August 2011, both at 20 m spatial resolution. Radiometric
31 normalization was performed using robust Theil-Sen regression on the overlap between the
32 two scenes to adjust the 2008 radiometry to match the 2011 image. The Enhancement

1 Classification Method (Beaubien et al., 1999) was used to improve image contrast by
2 stretching the dynamic range representing land features to the full 8-bit dynamic range while
3 compressing water, cloud and shadow. A large number of spectral clusters were generated
4 from the enhanced multispectral data using fuzzy *K*-means clustering and applying a pseudo-
5 colour table to represent the enhanced colours. The Classification by Progressive
6 Generalization approach (Cihlar et al., 1998) was used to manually merge and label clusters to
7 16 land-cover types considering spectral similarity and spatial proximity to depict land-cover
8 features visible in high resolution images in Google EarthTM and our field data. Validation of
9 a national land-cover product (Olthof et al., 2013) that includes this study area suggests an
10 overall accuracy in the range of 70 %. We modelled permafrost conditions for 13 land-cover
11 types, which exclude water, roads and recently disturbed areas (Table 1).

12 We estimated the probability distribution of the ground-types in each land-cover type using
13 field observations of OLT. Most of the land-cover types had five to eight ground-types (Table
14 2). Rock outcrop was assumed as one ground-type without organic layer. The parameters
15 were determined by fitting the observed relative cumulative frequency with the modified
16 logistic function (Table 2). Our field observations in the study area did not include land-cover
17 types of erect shrubs, shrub-herb mixture and herbs (types S, SH and H, respectively). To fill
18 this data gap, we used field observations of these land-cover types that were conducted in
19 2013 near Tuktoyaktuk (69.44° N, 133.03° W) and Fort McPherson (67.44° N, 134.88° W).
20 These observations may over-estimate the OLT in our study area, especially when bedrock is
21 near the surface.

22 2.2.3 Leaf area indices and fire disturbances

23 Leaf area indices in mid-summer (Fig. 3d) were mapped using Landsat-5 imagery (acquired
24 on 21 July 2002) based on Abuelgasim and Leblanc (2011), who developed an equation of
25 LAI using field observations and the reduced simple ratio index of Landsat channels 3, 4 and
26 5. As they normalized their Landsat scenes based on SPOT VGT composite in the summer of
27 2005, we first normalized our Landsat images to the same SPOT VGT composite and then
28 calculated LAI using their LAI equation.

29 A digital database of historically burned areas and year of burning (Fig. 3e) was obtained
30 from the Government of Northwest Territories Centre for Geomatics
31 (<http://www.geomatics.gov.nt.ca/>). In the study area, about 26.2 % of the land area

1 experienced wildfire since 1967. The major fires were in 1973 and 1998, which accounted for
2 71.6 % and 19.3 % of the total burned area, respectively. Fires consume vegetation and soil
3 organic matter. The amount of consumption and the post-fire regeneration process depend on
4 fire intensity, vegetation condition, soil moisture and local topography (Turetsky et al., 2011).
5 For simplicity, we assumed that fires consumed all the foliage, and the remaining standing
6 woody parts had little effect on radiation and surface energy exchanges. The albedo of the
7 land surface in snow-free period was reduced by 50 % immediately after the fire (Yoshikawa
8 et al., 2003; Mack et al., 2011). We assumed that fire could consume a maximum of 13 cm of
9 mosses and top organic matter except for wetland and fen (type W), where we used half of
10 this depth due to their wet conditions (Johnstone et al., 2010; Turetsky et al., 2011).

11 Although trees can take several decades to re-establish, the regeneration and re-establishment
12 of sedges and shrubs occur rapidly (Bond-Lamberty et al., 2002). Based on the LAI map for
13 this area (representing the conditions in 2002), the average LAI in the area burned after 1994
14 (mostly in 1998) was about 60 % of the average LAI in the non-burned area, and the average
15 LAI in the area burned before 1973 was about 120 % of the non-burned area. Based on these
16 results and other studies (Bond-Lamberty et al., 2002), we assumed that land-cover types
17 dominated by sedges and shrubs would regenerate in the following year after a fire and LAI
18 would reach pre-burn levels in 5 and 15 years, respectively. Tree-dominated land types would
19 regenerate in 5 years after a fire and LAI would reach pre-burn level in 50 years (Bond-
20 Lamberty et al., 2002). We also assumed that the surface organic matter and mosses
21 consumed by fire would recover in 50 years (Mack et al., 2011). The albedo of the land
22 surface would also return to the pre-burn level. The increases in LAI, albedo and surface
23 organic layer were treated as linear patterns with time after regeneration. After recovery, the
24 land-cover types will be the same as pre-burn conditions, and summer LAI will not change
25 with time (LAI varies seasonally). We did not consider new fires after 2013.

26 2.2.4 Climate data

27 The 5 arc-minutes (about 10 km) spatial 30 year averages (1971-2000) of monthly air
28 temperature (Fig. 3f) and precipitation were from McKenney et al. (2012). The data were
29 interpolated from station observations. We interpolated these monthly data to 20 m resolution
30 using bi-linear interpolation, and calculated annual total degree-days when air temperature
31 was above 0 °C. Based on annual total degree-days and annual total precipitation, the climate
32 was clustered into 20 classes. The average relative errors were 0.25 % and 0.45 % for the

1 annual total degree-days and annual total precipitation, respectively. Temporal climate
2 changes were estimated using daily observations at the Yellowknife airport climate station as
3 a template. A detailed description of the method can be found at Zhang et al. (2013). From the
4 1940s to the recent past decade (2003-2012), annual mean air temperature increased by 2.1
5 °C. The increase mainly occurred after the mid-1960s. Annual total precipitation increased by
6 99 mm from the 1940s to the past decade.

7 The climate scenario data were downloaded from the World Data Center for Climate
8 (<http://mud.dkrz.de/wdc-for-climate/> accessed in April 2011). First, we selected 18 climate
9 projections of six climate models (CCCma, ECHAM, HadCM, GFDL, MIROC and NRCAR)
10 under three greenhouse gas emissions scenarios (B1, A1B and A2), then we selected three
11 climate change scenarios to represent low, medium and high warming scenarios based on
12 their temperature projections. They were generated by CCCma (B1), CCCma (A1B) and
13 MIROC (A1B) (Fig. 4). We did not select CCCma (A2) because the projected air temperature
14 is lower than several other projections and it is similar and sometimes lower than that of
15 CCCma (A1B) before the 2050s. Under the selected three scenarios, air temperature is
16 projected to increase 0.4, 1.7 and 2.7 °C, respectively, from the recent past decade to the
17 2050s; and to increase 1.0, 3.4 and 4.9 °C, respectively, from the recent past decade to the
18 2090s. The projected changes in precipitation are not very significant (Fig. 4b).

19 2.2.5 Other input parameters

20 In addition to OLT, the model also requires inputs about mineral soil conditions and
21 hydrological parameters. Field surveys and coring indicate differences in sediment types
22 above and below an elevation of about 205 m above sea level (a.s.l.), likely related to
23 sedimentation within the glacial lake McConnell (Stevens et al., 2012). Therefore, we first
24 divided the study area into two regions using the 205 m a.s.l. isoline (Fig. 3b) and then
25 defined the mineral soil conditions for each region. This delineation also closely corresponds
26 to the separation of the Great Slave Lowlands and Uplands (Ecological Classification Group,
27 2007). At elevations below 205 m, mineral soils are mainly composed of clay (Wolfe et al.,
28 2011). Above 205 m., mineral soils were assigned as sandy loam for the low-vegetation or
29 barren land (type L) and low- to medium-density coniferous forest (type C3), and as silty clay
30 for other land-cover types based on the general patterns of field observations (Stevens et al.,
31 2012; Wolfe et al., 2011). The organic matter content in mineral soils was estimated based on
32 the general patterns observed by Hossain et al. (2007). Except for low vegetation and bedrock

(Types L and R), the depth of all surficial deposits (including peat and mineral soils) are assumed to be 7 m for bogs and wetlands (types C5 and W) and 5 m for other land types based on most of the borehole observations (Wolfe et al., 2011). The soil thickness for the low vegetation type was assumed to be 2.5 m and we assumed no soil on bedrock outcrops. The thermal conductivity of bedrock was $0.026 \text{ W m}^{-1} \text{ }^{\circ}\text{C}^{-1}$ (Brown, 1973). The depth of the ground profile simulated was 120 m, and heat flux at the bottom of the ground profile was assumed as 0.007 W m^{-2} (Majorowicz and Grasby, 2010).

The model also requires several parameters to estimate lateral water flows (Zhang et al., 2002, 2012). We defined these parameters based on the general drainage conditions and the range of water table for different land-cover types (Table 3). The model also has a parameter to consider the effects of snow-drifting due to wind (Zhang et al., 2012). A positive value is for the fraction of snowfall drifted away from the site and a negative value for capturing some drifting snow from surroundings. We estimated this parameter based on the vegetation types and their density (represented by the LAI in summer) (Table 3). Since this region is relatively flat, we did not consider the effects of topography on solar radiation.

2.2.6 Spatial modelling

To reduce the computation time, LAI was divided into 18 levels based on the effects of LAI on solar radiation (i.e., $\exp(-0.5\text{LAI})$). The latitude in the area was divided into five grads (0.2° difference between two adjacent grads). Together with the land-cover types (13 types), elevation levels (2 types), climate (20 classes), and wildfire years (13 types), the land pixels in the study area had 31 724 unique combinations of the input types, which was 0.2 % of the land pixels in this area (We ran the model only for these unique input types rather than running the model pixel by pixel). For each land-cover type, the model was run for all the ground-types under the three climate scenarios. Model computations took about three weeks using three personal computers.

3 Result and analysis

3.1 Permafrost distributions

Figure 5 shows the distributions of permafrost probability modelled for the 1950s (1950-1959), the 2000s (2000-2009) and the 2050s (2050-2059). These results show significant reductions in permafrost probability due to climate warming from the 1950s to the 2050s.

1 Permafrost is predicted to disappear completely in most of the area by the end of the 21st
2 century. The spatial distribution of permafrost in this area was mainly related to land-cover
3 types and associated ground conditions. For example, the non-permafrost area in the 2000s
4 mainly occurred in rock outcrops, low vegetation, and deciduous forest (Land-cover types R,
5 L and D, respectively), while sparse coniferous forest (types C4 and C5) and herb dominated
6 areas and wetlands (types H and W) had high permafrost probability. Leaf area indices and
7 fire disturbances also affected permafrost conditions, but their effects were mixed with that of
8 land-cover types. Permafrost probability in the northeast corner of the study area was higher,
9 probably due to the relatively cooler climate in this area. However, the overall effects of the
10 climate gradient on spatial distribution of permafrost were not so obvious because of the
11 strong effects of ground conditions and relatively small climate gradient in this area (Fig. 3f).
12 For example, although the southern part is slightly warmer than the northern part, LAI is
13 higher and soils contain more clay in the south, which compensated for the effects of warmer
14 temperature on permafrost development.

15 Figure 6a shows the modelled temporal change of average permafrost probability (or
16 permafrost extent) in this area from 1942 to 2100. On average, permafrost extent was reduced
17 from 72.0 % in the 1950s to 52.0 % in the 2000s. The model predicted that permafrost extent
18 would be reduced to 12.4 % in the 2050s and to 2.5 % in the 2090s. The difference in
19 permafrost extent between the low and high warming scenarios was relatively small, usually
20 less than 5 % (in permafrost extent).

21 Different land-cover types show different decreasing patterns in permafrost extent (Fig. 6b).
22 The most rapid reduction in permafrost extent was in low vegetation or barren land (type L)
23 due to their exposed land conditions. The reduction was rapid in deciduous forest area (type
24 D) due to its shallow OLT. Spruce lichen bogs and wetlands (types C5 and W) were the last
25 land-cover types experiencing permafrost reduction. With time, the reduction of permafrost
26 for a land-cover type generally shows a slow, rapid and slow decline pattern. The initial slow
27 reduction is due to the lower warming rate of climate (especially before the mid of the 1980s)
28 and the time required to warm the ground to a critical level. The later slow reduction of
29 permafrost is related to ground-types with deep organic layers and high LAI, which can
30 protect permafrost from thawing (Shur and Jorgenson, 2007). Model results show that some
31 forest areas could still maintain permafrost by the end of the 21st century mainly due to their

1 deep OLT and high LAI, assuming they were not disturbed by wildfires during the 21st
2 century.

3 **3.2 The most likely permafrost conditions**

4 Permafrost conditions under varying ground-types differ significantly due to the effects of
5 OLT. Permafrost does not typically exist where OLT is very shallow. Therefore it is difficult
6 to calculate the average permafrost conditions. A meaningful way is to present the most likely
7 permafrost conditions, which is determined from the model results of the most likely ground-
8 types under the medium warming climate scenario. The most likely permafrost extent
9 averaged in this area (dashed curve in Fig. 6a) was slightly different from the average of all
10 the ground-types under the three climate scenarios (solid curve in Fig. 6a). The average and
11 the most likely spatial patterns were similar in the 1950s and 2000s (the most likely
12 permafrost distribution only has two types, no permafrost or with permafrost, shown
13 respectively as white or other colours in Fig. 7). However, the average and the most likely
14 permafrost distributions were very different in the 2050s (comparing Figs. 5c and 7c) as
15 permafrost was predicted to disappear in most areas under the most probable ground and
16 climate conditions.

17 Figure 7 shows the distribution of the most likely active-layer thicknesses in the 1950s, 2000s
18 and 2050s. Active layer deepened from the 1950s to the 2000s, and permafrost in most areas
19 was predicted to disappear in the 2050s. The red patches (deeper active layer) in the
20 northeastern corner in Fig. 7b are due to the effects of wildfires, which consumed vegetation
21 and some of the top organic matters. For the pixels with permafrost in all the years before
22 2012, the average active-layer thickness increased from 0.7 m in the 1940s to 1.4 m in the
23 2000s.

24 **3.3 Result verification**

25 According to the Canada permafrost map (Heginbottom et al., 1995), the study area is within
26 the extensive discontinuous permafrost zone. Based on the 124 observation sites in this area,
27 permafrost was detected at 87 sites. Frozen ground was not detected at the other 37 sites. The
28 permafrost sites account for 70.2 % of the observation sites, which confirm that this area is
29 within the extensive discontinuous permafrost zone (50 – 90 %). The modelled average
30 permafrost extent in this area was 64.2 % during 1942-2012, well within the range of the

1 extensive discontinuous zone. Based on the ground-types most closely matching local
2 conditions, the model results show that permafrost occurred at 71 of 87 observed permafrost
3 sites. For the other 37 sites where no frozen ground was detected in the field, the model
4 results show that 21 sites did not have permafrost, six sites had permafrost but their thaw
5 depths were deeper than the measurement depths, and the model results were incorrect for the
6 other ten sites. Overall, the model correctly simulated permafrost occurrence for 82 % of the
7 observed permafrost sites, and correctly simulated 73 % of the sites where frozen ground was
8 not detected in the field either because thaw depths were deep, or permafrost did not exist.
9 Coincidentally, the modelled and observed total numbers of sites with permafrost (87 sites)
10 were the same.

11 Figure 8a shows a comparison between the modelled and observed percentage of sites with
12 permafrost at each land-cover type. The model results were close to the observations for most
13 of the land-cover types except for the low vegetation sites (L). Permafrost was observed at
14 three of the four low vegetation sites whereas the model did not indicate permafrost at these
15 sites. Field data show that two sites are in disturbed areas with some peat layers added in the
16 soil profile and another site is near the road with some embankment material on the surface.
17 These modified conditions may have actually promoted permafrost development.

18 Wolfe et al. (2014) identified 955 lithalsas in our study area (Fig. 3b). By definition,
19 permafrost exists at these locations. We calculated the average permafrost probability during
20 1978-1980, at which time the aerial photographs were acquired to identify the lithalsas.
21 Eighteen locations were classified as water since they are very close to water bodies. The
22 model results show that all the 937 non-water locations have a ≥ 14 % probability of
23 permafrost occurrence. The probability of permafrost occurrence was ≥ 50 % at 838 locations,
24 and was ≥ 90 % at 501 locations. The average probability was 76.9 % for all the locations.
25 The lithalsa mounds are usually well drained due to their local topography and contain
26 segregation ice. The modelled did not consider these factors therefore they might contribute to
27 the underestimation of the probability of permafrost occurrence for these locations.

28 The modelled mean summer thaw depth for each land-cover type was comparable with the
29 observations although the variation range was usually large among the sites (Fig. 8b). The
30 modelled average thaw depth of all the sites with permafrost was 0.78 m, which was very
31 close to the average of the observations (0.81 m). Figure 9 shows a scatter graph comparison
32 for the 71 sites with permafrost. The magnitudes of the modelled summer thaw depths were

1 similar to the observations for most of the sites although significant differences existed for
2 some sites due to their specific soil, vegetation and hydrological conditions. The correlation
3 coefficient is 0.365 ($n = 71$).

4 The modelled dynamics of snow depth, especially the timing of accumulation and
5 disappearance of snow and the maximum snow depth, compared well with the observations at
6 the Yellowknife climate station. The correlation coefficient is 0.892 for the 19794
7 observations from the 1955 to 2012. The modelled permafrost thickness for recent decades
8 ranged from several metres to 130 m, which is comparable with the observations reported by
9 Smith and Burgess (2002) and Roujanski et al. (2012). We also tested the model offline using
10 observations in this area measured by Brown (1973), Karunaratne et al. (2008), and Roujanski
11 et al. (2012). Based on their local ground and vegetation conditions, the model could capture
12 their ground temperature regimes and permafrost conditions.

13 **4 Discussion**

14 This study proposes a new approach for mapping permafrost and change with climate
15 considering uncertainties in ground conditions and climate projections. We apply this
16 approach at 20 m resolution to a large area in northern Canada. The data requirement and the
17 cost of computation are reasonable, and the mapped permafrost conditions are in reasonable
18 agreement with field observations and other studies. Compared to previous mapping methods,
19 several features of this approach are noteworthy.

20 First, compared to the traditional zonal permafrost mapping methods (Nikiforoff, 1928;
21 Heginbottom et al., 1995; Brown et al., 1998), this new approach is more objective,
22 replicable, and quantitative in integrating most of the related factors, and can be used to map
23 permafrost at higher spatial resolution and to assess the impacts of climate change. Unlike the
24 equilibrium models (Riseborough et al., 2008), our process-based modelling approach can
25 quantify the transient responses of permafrost to changes in climate and ecosystems.

26 Second, this approach integrates satellite remote sensing data, field observations, and a
27 process-based model. Satellite data can greatly improve the spatial resolution of existing
28 permafrost maps, and can provide various parameters including land-cover, LAI, wildfire, and
29 topographic features. As current soil and surficial geological maps are coarse, the
30 heterogeneous ground conditions are statistically represented based on field observations.

1 Third, the produced permafrost maps by this approach are more useful for land-use planners
2 and decision-makers due to their higher spatial resolution and effectively incorporating
3 incomplete and uncertain information about ground conditions and future climate projections.
4 Previous studies usually presented different permafrost maps under assumed different ground
5 conditions and climate change scenarios (e.g., Zhang, 2013; Zhang et al., 2008, 2013; Daanen
6 et al., 2011). Such results are difficult to use due to their wide differences. This probability
7 concept is similar to the traditional permafrost maps, but the new approach can develop
8 permafrost maps with a much higher degree of precision and spatial resolution. Figure 10
9 shows the importance of spatial resolution for permafrost zones. At 20 km resolution, our
10 results show the same permafrost zone as in the traditional permafrost map (extensive
11 discontinuous). At finer resolutions, however, other permafrost zones appeared. In addition,
12 this approach also provides most likely permafrost conditions, such as active-layer thickness
13 and permafrost thickness.

14 Finally, this approach may serve as a practical way to map permafrost evolution at high
15 spatial resolution for other regions. Satellite remote sensing data are routinely available across
16 the globe. To consider the heterogeneity of ground conditions, we estimated their statistical
17 distributions rather than mapping ground conditions explicitly, which is difficult at present.
18 Organic layer thickness and other general ground conditions can be surveyed in the field and
19 the data can be accumulated gradually as they do not change significantly with time without
20 disturbances. In this study, we estimated the probability of ground-types based on OLT. With
21 more field data available, other ground features can be included to better define ground-types.
22 The spatial input data can be organized and used to run the model on multiple computers
23 simultaneously, thus greatly reducing computation time for high resolution spatial modelling.
24 In addition, this approach allows for changes or improvement in spatial resolution, new
25 development in the model and remote sensing technology, and with the availability of more
26 field observations.

27 Permafrost is a ground thermal condition influenced by many factors of geological, climatic,
28 hydrological and ecological processes at different temporal and spatial scales (Jorgenson et
29 al., 2010; Shur and Jorgenson, 2007; Bonnaventure and Lamoureux, 2013). Although our new
30 mapping approach quantitatively integrated most of the factors based on energy and water
31 dynamics, it has several limitations. First, the NEST model is one-dimensional and assumes
32 each grid cell to be uniform without lateral heat exchange. Therefore the results cannot

1 represent areas with strong lateral heat fluxes, such as areas between very different land-cover
2 types, especially close to water bodies. And the model does not consider permafrost thaw due
3 to lateral heat flow, which could be important for patchy permafrost. Second, we considered
4 fire disturbances occurred in the past, but we did not consider future fires. Such a treatment
5 might over-estimate future permafrost extent because high LAI and deep organic layer can
6 effectively keep permafrost in disequilibrium from the warming of the atmospheric climate
7 (Camill and Clark, 1998; Shur and Jorgenson, 2007). Ground subsidence and related
8 hydrological changes could have significant impacts on permafrost degradation as well. And
9 finally, this study did not consider changes in land-cover types and LAI with climate
10 warming. Observations show that northern high latitudes are becoming greener and shrubbier
11 with climate warming (e.g., Tape et al., 2006). These changes can be very important for the
12 evolution of permafrost.

13 **5 Conclusions**

14 Spatially detailed information about permafrost evolution with climate warming is important
15 for land-use planning and for environmental and ecological assessments. Although satellite
16 remote sensing can provide detailed maps of vegetation and land-cover types, knowledge
17 regarding soil and ground conditions are much coarser, which greatly limits our capacity to
18 map permafrost at higher resolutions. The wide range of projected climate scenarios also
19 brings in uncertainties for mapping permafrost change. Our proposed new approach
20 incorporates these uncertainties for permafrost mapping by integrating remote sensing, field
21 observations, and a process-based model. Land-cover types from satellite remote sensing are
22 used to capture the general land features and to improve the spatial resolution of existing
23 permafrost maps. Other vegetation features can also be derived from remote sensing imagery.
24 The probability of different ground conditions within land-cover types is estimated from field
25 observations. A process-based model is used to quantify the dynamics of permafrost for each
26 ground-type under three representative climate scenarios of low, medium and high warming.
27 From the model results, the probability of permafrost occurrence and the most likely
28 permafrost conditions are determined. We apply this approach at 20 m resolution to a large
29 area in Canada. The mapped permafrost conditions are in agreement with field observations
30 and other studies. This demonstrates that the data requirements, model robustness and
31 computation time are reasonable, and that this approach may serve as a practical means to
32 map permafrost evolution at a high resolution in other regions.

1
2
3
4
5
6
7
8
9
10
11
12

Acknowledgements

The authors would like to thank Sylvain Leblanc for providing software and procedures for mapping leaf area indices, and undertaking the critical internal review of the paper. Adrian Gaanderse provided many site observations about ground conditions in the study area. The authors also thank Peter Morse and two anonymous reviewers for carefully reviewing the paper. This study was supported by the Climate Change Geoscience Program and Remote Sensing Science Program in Natural Resources Canada (Earth Science Sector contribution number 20130435), and Cumulative Impact Monitoring Program (CIMP) in Northwest Territories, Canada.

References

- ACIA: Impact of a Warming Arctic: Arctic Climate Impact Assessment, Cambridge University Press, 1042 pp., 2005.
- Abuelgasim, A. A. and Leblanc, L.: Leaf area index mapping in northern Canada, *International Journal of Remote Sensing*, 32, 5059-5076, doi: 10.1080/01431161.2010.494636, 2011.
- Anisimov, O. A. and Nelson, F. E.: Permafrost zonation and climate change: results from transient general circulation models, *Climatic Change*, 35, 241–258, 1997.
- Anisimov, O. and Reneva, S.: Permafrost and changing climate: The Russian perspective, *Ambio*, 35, 169-175, 2006.
- Beaubien, J., Cihlar, J., Simard, G., and Latifovic, R.: Land cover from multiple Thematic Mapper scenes using a new enhancement-classification methodology, *Journal of Geophysical Research*, 104, D22, 27909-27920, 1999.
- Bond-Lamberty, B., Wang, C., Gower, S. T., and Norman, J.: Leaf area dynamics of a boreal black spruce chronosequence, *Tree Physiology*, 22, 993-1001, 2002.
- Bonnaventure, P. P. and Lamoureux, S. F.: The active layer: a conceptual review of monitoring, modelling techniques and changes in a warming climate, *Prog. Phys. Geogr.*, 37, 352–376, doi: 10.1177/0309133313478314, 2013.
- Bonnaventure, P. P. and Lewkowicz, A. G.: Impacts of mean annual air temperature change on a regional permafrost probability model for the southern Yukon and northern British Columbia, Canada, *The Cryosphere*, 7: 935-946, doi: 10.5194/tc-7-935-2013, 2013.
- Bonnaventure, P. P., Lewkowicz, A. G., Kremer, M., and Sawada, M. C.: A permafrost probability model for the southern Yukon and northern British Columbia, Canada, *Permafrost and Periglacial Processes*, 23, 52–68, doi: 10.1002/ppp.1733, 2012.
- Brown, R. J. E.: Influence of climatic and terrain factors on ground temperatures at three locations in the permafrost region in Canada. *Proceedings of the second International Conference on permafrost, North American Contribution, Yakutsk, U. S. S. R., 27-34, July 13-18, 1973.*

1 Brown, J., Ferrians, Jr., O. J., Heginbottom, J. A., and Melnikov, E. S.: Circum-arctic map of
 2 permafrost and ground ice conditions, Boulder, CO, National Snow and Ice Data Center.
 3 Revised February 2001, Digital media, 1998.

4 Camill, P. and Clark, J. S.: Climate change disequilibrium of boreal permafrost peatlands
 5 caused by local processes, *The American Naturalist*, 151, 207-22, doi: 10.1086/286112, 1998.

6 Cihlar, J., Xiao, Q., Chen, J., Beaubien, J., Fung, K., and Latifovic, R.: Classification by
 7 progressive generalization: a new automated methodology for remote sensing multichannel
 8 data, *International Journal of Remote Sensing*, 19, 2685-2704, 1998.

9 Daanen, R. P., Ingeman-Nielsen, T., Marchenko, S. S., Romanovsky, V. E., Foged, N.,
 10 Stendel, M., Christensen, J. H., and Hornbech Svendsen, K.: Permafrost degradation risk zone
 11 assessment using simulation models, *The Cryosphere*, 5, 1043-1056, doi: 10.5194/tc-5-1043-
 12 2011, 2011.

13 Duchesne, C., and Wright, J. F., and Ednie, M.: High-resolution numerical modeling of
 14 climate change impacts on permafrost in the vicinities of Inuvik, Norman Wells, and Fort
 15 Simpson, NT, Canada. In: proceedings of the Ninth International Conference on Permafrost,
 16 29 June – 3 July 2008, Fairbanks, Alaska, USA, edited by Kane D. L. and Hinkel K. M.,
 17 Institute of Northern Engineering, University of Alaska Fairbanks, 385-390, 2008.

18 Duguay, C. R., Zhang, T., Leverington, D. W., Romanovsk, V. E.: Satellite remote sensing of
 19 permafrost and seasonally frozen ground, In: *Remote Sensing of Northern Hydrology*,
 20 *Geophysical Monograph Series 163*, Edited by Duguay C. R. and Pietroniro A., American
 21 Geophysical Union, Washington, doi: 10.1029/163GM06, 91-118 pp, 2005.

22 Ecosystem Classification Group: Ecological Regions on the Northwest Territories: Taiga
 23 Shield. Department of Environment and Natural Resources, Government of the Northwest
 24 Territories, Yellowknife, NT, Canada, 173 pp., 2007 (revised 2009).

25 Gaanderse, A.: Seasonal thaw depths in relation to surficial characteristics in the taiga shield
 26 high boreal ecoregion surrounding Yellowknife, Northwest Territories. A theses for a
 27 Bachelor's of Arts degree, Department of Geography and Environmental Studies, Carleton
 28 University, Ottawa, Canada, 59 pp., 2011.

29 Gruber, S.: Derivation and analysis of a high-resolution estimate of global permafrost
 30 zonation, *The Cryosphere*, 6 221-233, doi: 10.5194/tc-6-221-2012, 2012.

1 Haeberli, W.: Die Basistemperatur der winterlichen Schneedecke als möglicher Indikator für
2 die Verbreitung von Permafrost in den Alpen. Zeitschrift für Gletscherkunde und
3 Glazialgeologie, 1–2: 221–227, 1973.

4 Heginbottom, J. A., Dubreuil, M. A., and Harker, P. A.: Canada - Permafrost, in: National
5 Atlas of Canada, 5th edition, National Atlas Information Service, Natural Resources Canada,
6 Ottawa, ON, Canada, MCR 4177, 1995.

7 Heginbottom, J. A.: Permafrost mapping: a review, progress in Physical Geography, 26, 623-
8 642, doi: 10.1191/0309133302pp355ra, 2002.

9 Hossain, M. F., Zhang, Y., Chen, W., Wang, J., and Pavlic, G.: Soil organic carbon content in
10 northern Canada: A database of field measurements and its analysis, Canadian Journal of Soil
11 Science, 87, 259-268, doi: 10.4141/S06-029, 2007.

12 Harris, S. A.: Influence of organic (O_f) layer thickness in active-layer thickness at two sites in
13 the western Canadian arctic subarctic, Erdkunde, 41, 275-285, 1987.

14 Jafarov, E. E., Marchenko, S. S., and Romanovsky, V. E.: Numerical modeling of permafrost
15 dynamics in Alaska using a high spatial resolution dataset, The Cryosphere, 6, 613-624,
16 doi:10.5194/tc-6-613-2012, 2012.

17 Johnson, K. D., Harden, J. W., McGuire, A. D., Clark, M., Yuan, F. M., and Finley, A.:
18 Permafrost and organic layer interactions over a climate gradient in a discontinuous
19 permafrost zone, Environmental Research Letters, 8, 035028, doi: 10.1088/1748-
20 9326/8/3/035028, 2013.

21 Johnstone, J. F., Chapin III, F. S., Hollingsworth, T. N., Mack, M. C., Romanovsky, V., and
22 Turetsky, M.: Fire, climate change, and forest resilience in interior Alaska, Canadian Journal
23 of Forest Research, 40, 1302–1312, doi: 10.1139/X10-061, 2010.

24 Jorgenson, M. T., Romanovsky, V., Harden, J., Shur, Y., O'Donnell, J., Schuur, E. A. G.,
25 Kanevskiy, M., and Marchenko, S.: Resilience and vulnerability of permafrost to climate
26 change, Canadian Journal of Forest Research, 40: 1219-1236, doi: 10.1139/X10-060, 2010.

27 Karunaratne, K. C., Kokelj, S. V., and Burn, C. R.: Near-surface permafrost conditions near
28 Yellowknife, Northwest Territories, Canada. In the Ninth International Conference on
29 Permafrost, edited by Kane D. L. and Hinkel K. M., Institute of Northern Engineering,
30 University of Alaska Fairbanks, 907-912, 2008.

1 Kasischke, E. S. and Johnstone, J. F.: Variation in postfire organic layer thickness in a black
2 spruce forest complex in interior Alaska and its effects on soil temperature and moisture,
3 Canadian Journal of Forest Research, 35, 2164–2177, doi: 10.1139/X05-159, 2005.

4 Leverington, D. W. and Duguay, C. R.: A Neural network method to determine the presence
5 or absence of Permafrost near Mayo, Yukon Territory, Canada, Permafrost and Periglacial
6 Processes 8: 205–215, 1997.

7 Lawrence, D. M. and Slater, A.: A projection of severe near-surface permafrost degradation
8 during the 21st century, Geophysical Research Letters, 32, L24401,
9 doi: 10.1029/2005GL025080, 2005.

10 Lewkowicz, A. G. and Ednie, M.: Probability mapping of mountain permafrost using the BTS
11 method, Wolf Creek, Yukon Territory, Canada, Permafrost and Periglacial Processes, 15, 67–
12 80, doi:10.1002/ppp.480, 2004.

13 Mack, M. C., Bret-Harte, M. S., Hollingsworth, T. N., Jandt, R. R., Schuur, E. A. G., Shaver
14 G. R., Verbyla, D. L.: Carbon loss from an unprecedented Arctic tundra wildfire, Nature, 475,
15 489-492, doi: 10.1038/nature10283, 2011.

16 Majorowicz, J. and Grasby, S. E.: Heat flow, depth-temperature variations and stored thermal
17 energy for enhanced geothermal systems in Canada, Journal of Geophysics and Engineering,
18 7, 232-241, doi:10.1088/1742-2132/7/3/002, 2010.

19 Marchenko, S., Romanovsky, V., and Tipenko, G.: Numerical modeling of spatial permafrost
20 dynamics in Alaska, In: Proceedings of the Ninth International Conference on Permafrost, 29
21 June- 3 July 2008, Fairbanks, Alaska, USA, edited by Kane D. L. and Hinkel K. M., Institute
22 of Northern Engineering, University of Alaska, Fairbanks, 190-204, 2008.

23 Morrissey, L. A., Strong, L., and Card, D. H.: Mapping permafrost in the boreal forest with
24 Thematic Mapper satellite data, Photogrammetric Engineering and Remote Sensing, 52:
25 1513–1520, 1986.

26 Morse, P. D., Burn, C. R., and Kokelj, S. V.: Influence of snow on near-surface ground
27 temperatures in upland and alluvial environments of the outer Mackenzie Delta, Northwest
28 Territories, Canadian Journal of Earth Sciences, 49, 895-913, doi: 10.1139/E2012-012, 2012.

29 McKenney, D. W., Hutchinson, M. F., Papadopol, P., Lawrence, K., Pedlar, J., Campbell, K.,
30 Milewska, E. M., Hopkinson, R. F., Price, D., and Owen, T.: Customized Spatial Climate

1 Models for North America, *Bulletin of the American Meteorological Society*, 92, 1611-1622,
2 2011.

3 Nelson, F. E.: Permafrost zonation in eastern Canada: a review of published maps, *Physical*
4 *Geography*, 10, 233-248, 1989.

5 Nelson, F. E., and Outcalt, S. I.: A frost index number for spatial prediction of ground-frost
6 zones, In: *Permafrost-Fourth International Conference Proceedings*, vol. I, National Academy
7 Press, Washington, DC, pp. 907–911, 1983.

8 Nelson, F. E. and Outcalt, S. I.: A computational method for prediction and regionalization of
9 permafrost, *Arctic and Alpine Research*, 19, 279–288, 1987.

10 Nelson, F. E., Shiklomanov, G. N. I., Mueller, G., Hinkel, K. M., Walker, D. A. and
11 Bockheim, J. G. Estimating active-layer thickness over a large region: Kuparuk River basin,
12 Alaska, U. S. A., *Arctic and Alpine Research*, 29, 367-378, 1997.

13 Nguyen, T-N, Burn, C. R., King, D. J., and Smith, S. L.: Estimating the extent of near-surface
14 permafrost using remote sensing, *Mackenzie Delta, Northwest Territories, Permafrost and*
15 *Periglacial Processes*, 20, 141–153, doi: 10.1002/ppp.637, 2009.

16 Nikiforoff, C.: The perpetually frozen subsoil of Siberia, *Soil Science*, 26, 61-78, 1928.

17 Osterkamp, T. E.: The recent warming of permafrost in Alaska, *Global and Planetary Change*,
18 49, 187-202, doi: 10.1016/j.gloplacha.2005.09.001, 2005.

19 Olthof, I., Latifovic, R., and Pouliot, D.: National scale medium resolution land cover
20 mapping of Canada from SPOT 4/5 data, 34th Canadian Symposium on Remote Sensing,
21 Victoria, British Columbia, Canada, August 27-29, 2013.

22 Reger, R. D. and Solie, D. N.: Reconnaissance interpretation of permafrost, Alaska Highway
23 Corridor, Delta Junction to Dot Lake, Alaska: Alaska Division of Geological and Geophysical
24 Surveys Preliminary Interpretation Report 2008-3c, 10p., 2 sheets, scale 1:63,360, 2008.

25 Riseborough, D. W., Wolfe, S. A., and Duchesne, C.: Permafrost modelling in northern Great
26 Slave region Northwest Territories, Phase 1: Climate data evaluation and 1-D sensitivity
27 analysis, Geological Survey of Canada Open File 7333, 43 pp., Ottawa, ON, Canada, 2013.

28 Roujanski, V. E., Horne, B., Zhang, G., McGuaig, M. Blade, M. and Regular, M.: Warming
29 permafrost temperature at two mine sites in the North Slave Region, Northwest Territories,
30 Canada, In *Proceedings of the Tenth International Conference on Permafrost*, Vol. 1:

1 International contributions, 25 - 29 June 2012, Salekhard, Yamal-Nenets Autonomous
2 District, Russia, Edited by Hinkel K. M., The northern Publisher, Salekhard, Russia, 353-358,
3 2012.

4 Shiklomanov, N. I.: From exploration to systematic investigation: development of
5 geocryology in 19th- and early-20th-century Russia, *Physical geography*, 26, 249-263, 2005.

6 Smith, M. W., and Riseborough, D. W.: Ground temperature monitoring and detection of
7 climate change, *Permafrost and Periglacial Processes*, 7, 301–310, 1996.

8 Smith, S. L., and Burgess, M. M.: A digital database of permafrost thickness in Canada,
9 Geological Survey of Canada Open File 4173, 38 pp., Ottawa, ON, Canada, 2002.

10 Stevens, C. W., Wolfe, S. A., Gaanderse, A. J. R.: Lithalsa distribution, morphology and
11 landscape associations in the Great Slave Lowlands, Northwest Territories, Geological Survey
12 of Canada Open File 7255, 34 pp., Ottawa, ON, Canada, 2012.

13 Shur, Y. and Jorgenson, M. T.: Patterns of permafrost formation and degradation in relation to
14 climate and ecosystems. *Permafrost and Periglacial Processes*, 18: 7-19, 2007, DOI:
15 10.1002/ppp.582.

16 Tape, K., Sturm, M., and Racine, C.: The evidence for shrub expansion in Northern Alaska
17 and the Pan-Arctic, *Global Change Biology*, 12, 686–702, doi: 10.1111/j.1365-
18 2486.2006.01128.x, 2006.

19 Turetsky, M. R., Kane, E. S., Harden, J. W., Ottmar, R. D., Manies, K. L., Hoy, E., and
20 Kasischke, E. E.: Recent acceleration of biomass burning and carbon losses in Alaskan forests
21 and peatlands, *Nature Geoscience*, 4, 27-31, doi:10.1038/ngeo1027, 2011.

22 Vaughan, D. G., Comiso, J. C., Allison, I., Carrasco, J., Kaser, G., Kwok, R., Mote, P.,
23 Murray, T., Paul, F., Ren, J., Rignot, E., Solomina, O., Steffen, K., and Zhang, T.:
24 Observations: Cryosphere, In: *Climate Change 2013: The Physical Science Basis*.
25 Contribution of Working Group I to the Fifth Assessment Report of the Intergovernmental
26 Panel on Climate Change, Edited by Stocker, T. F., Qin, D., Plattner, G.-K., Tignor, M.,
27 Allen, S. K., Boschung, J., Nauels, A., Xia, Y., Bex, V., and Midgley, P. M., Cambridge
28 University Press, Cambridge, United Kingdom, and New York, NY, U.S.A., 317-382 pp.
29 2013.

- 1 Vitt, D. H., Halsey, L. A., and Zoltai, S. C.: The bog landforms of continental western Canada
2 in relation to climate and permafrost patterns, *Arctic and Alpine Research*, 26, 1-13, 1994.
- 3 Wang, T., Hamann, A., Spittlehouse, D., and Aitken, S. N.: Development of scale-free
4 climate data for western Canada for use in resource management, *International Journal of*
5 *Climatology*, 26, 383-397, doi: 10.1002/joc.1247, 2006.
- 6 Wild, G. O.: Air Temperature in the Russian Empire. St Petersburg, Russia: Izdatel'stvo
7 Russkogo Geograficheskogo Obshestva. In Russian, 1882.
- 8 Wolfe, S. A., Duchesne, C., Gaanderse, A., Houben, A. J., D'Onofrio, R. E., Kokelj, S. V.,
9 and Stevens, C. W.: Report on 2010-2011 Permafrost Investigations in the Yellowknife Area,
10 Northwest Territories, Geological Survey of Canada Open File 6983, Ottawa, ON, Canada, 75
11 pp., 2011.
- 12 Wolfe, S. A., Stevens, C. W., Gaanderse, A. J., and Oldenborger, G. A.: Lithalsa distribution,
13 morphology and landscape associations in the Great Slave Lowland, Northwest Territories,
14 Canada, *Geomorphology*, 204, 302-313, doi: 10.1016/j.geomorph.2013.08.014, 2014.
- 15 Woo, M., Lewkowicz, A. G., and Rouse, W. R.: Response of the Canadian permafrost
16 environment to climatic change, *Physical geography*, 13, 287-317, 1992.
- 17 Wright, J. F., Duchesne, C., and Côté, M. M.: Regional-scale permafrost mapping using the
18 TTOP ground temperature model, In: *Proceedings of the 8th International Conference on*
19 *Permafrost*, Zurich, Switzerland, 21-25 July 2003, edited by Philips, M., Springman, S. M.,
20 and Arenson, L. U., 1241-1246, 2003.
- 21 Yi, S., Woo, M.-K., and Arain, A. M.: Impacts of peat and vegetation on permafrost
22 degradation under climate warming, *Geophysical Research Letters*, 34, L16504, doi:
23 10.1029/2007GL030550, 2007.
- 24 Yoshikawa, K., Bolton, W. R., Romanovsky, V. E., Fukuda, M., and Hinzman, L. D.: Impacts
25 of wildfire on the permafrost in the boreal forests of interior Alaska, *Journal of Geophysical*
26 *Research*, 107, 8184, doi: 10.1029/2001JD000438, 2003.
- 27 Zhang, T., Barry, R. G., Knowles, K., Heginbottom, J. A., and Brown, J.: Statistics and
28 characteristics of permafrost and ground ice distribution in the Northern Hemisphere, *Polar*
29 *Geography*, 23, 147-169, 1999.

1 Zhang, Y.: Spatio-temporal features of permafrost thaw projected from long-term high
2 resolution modeling for a region in the Hudson Bay Lowlands in Canada, *Journal of*
3 *Geophysical Research-Earth Surface*, 118, 542-552, doi: 10.1002/jgrf.20045, 2013.

4 Zhang, Y., Li, C., Trettin, C. C., Li, H., and Sun, G.: An integrated model of soil, hydrology
5 and vegetation for carbon dynamics in wetland ecosystems, *Global Biogeochemical Cycles*,
6 16, 1061, doi: 10.1029/2001GB001838, 2002.

7 Zhang, Y., Chen, W., and Cihlar, J.: A process-based model for quantifying the impact of
8 climate change on permafrost thermal regimes, *Journal of Geophysical Research*, 108(D22),
9 4695, doi: 10.1029/2002JD003354, 2003.

10 Zhang, Y., Chen, W., Smith, S. L., Riseborough, D. W., and Cihlar, J.: Soil temperature in
11 Canada during the twentieth century: complex responses to atmospheric climate change,
12 *Journal of Geophysical Research*, 110, D03112, doi: 10.1029/2004JD004910, 2005.

13 Zhang, Y., Chen, W., and Riseborough, D. W.: Temporal and spatial changes of permafrost in
14 Canada since the end of the Little Ice Age, *Journal of Geophysical Research*, 111, D22103,
15 doi: 10.1029/2006JD007284, 2006.

16 Zhang, Y., Chen, W., and Riseborough, D. W.: Disequilibrium response of permafrost thaw to
17 climate warming in Canada over 1850-2100, *Geophysical Research Letters*, 35, L02502, doi:
18 10.1029/2007GL032117, 2008.

19 Zhang, Y., Li, J., Wang, X., Chen, W., Sladen, W., Dyke, L., Dredge, L., Poitevin, J.,
20 McLennan, D., Stewart, H., Kowalchuk, S., Wu, W., Kershaw, G. P., and Brook, R. K.:
21 Modelling and mapping permafrost at high spatial resolution in Wapusk National Park,
22 Hudson Bay Lowlands, *Canadian Journal of Earth Sciences*, 49, 925-937, doi:
23 10.1139/E2012-031, 2012.

24 Zhang, Y., Wang, W., Fraser, R., Olthof, I., Chen, W., McLennan, D., Ponomarenko, S., and
25 Wu, W.: Modelling and mapping climate change impacts on permafrost at high spatial
26 resolution for an Arctic region with complex terrain, *The Cryosphere*, 7, 1121-1137,
27 doi:10.5194/tc-7-1121-2013, 2013.

28

1 Table 1 Land-cover types classified using SPOT satellite

Code	Name	Type description
D	Deciduous - medium to high density	Cold deciduous forest, closed tree canopy (crown closure 25-60%), small coniferous-herb understory.
M	Mixed - medium to high density	Mixed cold deciduous-needle leaved evergreen forest (crown closure 25-50%).
C1	Coniferous - high density	Sub-polar needle leaved evergreen forest (crown closure >75%).
C2	Coniferous - medium density	Sub-polar needle leaved evergreen forest, lichen-shrub understory.
C3	Coniferous - low to medium density	Sub-polar needle leaved evergreen forest, low-medium density, shrub-lichen understory.
C4	Sparse coniferous forest-shrub cover	Sparse needle leaved evergreen forest, herb-shrub cover understory.
C5	Spruce lichen bog	Wetland type feature that supports lichens and treed bogs.
W	Wetland or fen	Treed or herbaceous wetland with water table near or above the surface.
S	Erect shrubs	Tall shrubs or dense low shrubs.
SH	Shrub-herb mixture	Mixture of herbs and shrubs.
H	Herbs	Herb dominated (but not fens)
L	Low vegetation or lichen barren	Low- or non-vegetated area (but not roads or recently disturbed areas).
R	Rock outcrop	Rock outcrops with sparse vegetation.
U	Disturbed area	Recently disturbed areas (not modelled)
O	Roads	Roads (not modelled)
W	Water	Lakes, rivers, or ponds (not modeled)

2

3

1 Table 2 Probability parameters of organic layer thickness and the number of ground-types for
2 each land-cover type estimated using field observations.

Type code	Observa- tion sites	Probability parameters (cm)			R^2	Number of ground-types
		x_0	μ	s		
D	9	0.0	1.0	4.5	0.983	5
M	16	0.0	2.0	9.5	0.970	6
C1	15	0.0	10.8	2.5	0.963	5
C2	14	0.0	16.0	11.0	0.989	7
C3	7	0.0	13.0	9.5	0.949	6
C4	6	0.0	27.0	17.0	0.952	7
C5	20	20.1	80.0	26.0	0.980	8
W	25	5.2	31.0	16.0	0.970	7
S	19	2.7	10.0	8.0	0.956	7
SH	11	0.0	10.0	8.0	0.999	7
H	6	9.4	17.0	4.0	0.959	7
L	4	0.0	0.2	0.5	0.831	3
R	8	-	-	-	-	1

3 R^2 is the square of the correlation coefficient between the fitted and observed relative
4 cumulative frequency.

5

1 Table 3. Hydrological parameters defined for different land-cover types

Type code	Ground inflow		Surface outflow		Ground outflow		Snow drifting parameter
	WT_{ig}	F_{ig}	WT_{os}	F_{os}	WT_{og}	F_{og}	
D	100	0.1	0	0.1	50	0.05	0
M	100	0.1	0	0.1	30	0.05	-0.03L
C1	–	–	10	0.1	30	0.05	-0.05L
C2	–	–	0	0.1	30	0.05	-0.03L
C3	–	–	0	0.1	30	0.05	0.00
C4	–	–	0	0.1	30	0.02	0.00
C5	60	0.1	0	0.1	20	0.05	0.00
W	20	0.05	-10	0.05	-	-	0.00
S	–	–	0	0.1	20	0.1	-0.10L
SH	–	–	0	0.1	15	0.1	-0.05L
H	–	–	0	0.1	5	0.1	0.00
L	–	–	0	0.1	20	0.1	0.1-0.1L
R	–	–	0	0.5	–	–	0.2-0.1L

2 WT_{ig} is the lowest water table (cm below the surface) for beginning lateral ground inflow.
3 WT_{os} and WT_{og} are the highest water table (cm below the surface) for beginning lateral surface
4 and ground outflows, respectively. F_{ig} is the rate of ground inflow (day^{-1}). F_{os} and F_{og} are the
5 rates of surface and ground outflows, respectively (day^{-1}). Detailed description of these
6 parameters can be found in Zhang et al. (2002, 2012).

7 – is assuming no lateral flows.

8 L is for leaf area indices in peak growing season.

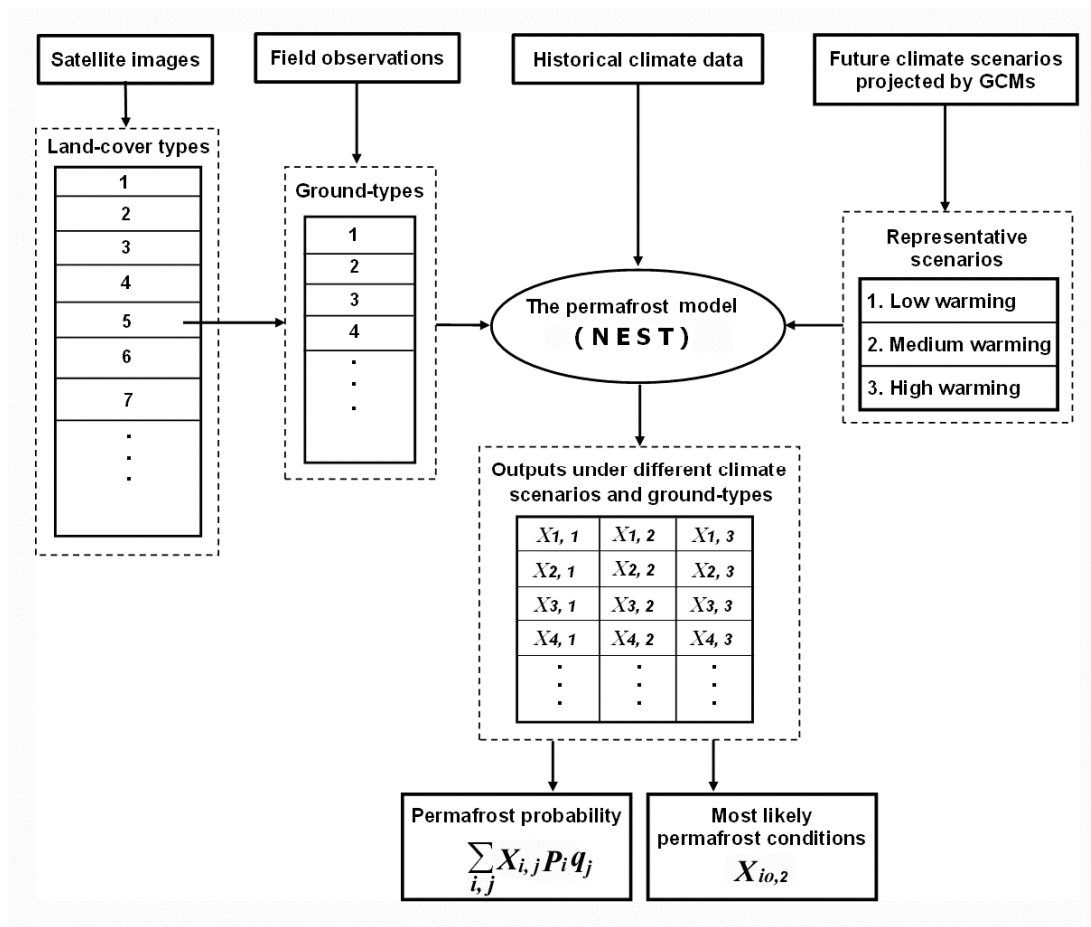
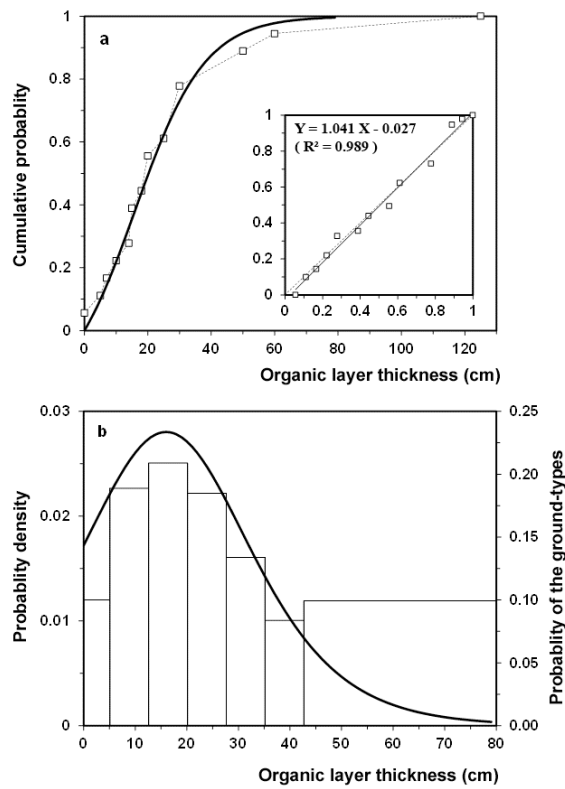


Figure 1. The scheme of the new permafrost mapping approach. A land-cover map classified from satellite images is used to represent the general land conditions and to improve the spatial resolution. For each land-cover type, the probability of different ground conditions is estimated based on field observations. A process-based permafrost model (NEST) was used to calculate the evolution of permafrost for each ground-type under three representative climate change scenarios generated by general circulation models (GCMs). From the model outputs, the probability of permafrost occurrence and the most likely permafrost conditions are determined. In the above scheme, $X_{i,j}$ is the model output based on ground-type i and climate scenario j . p_i is the probability of ground-type i , and q_j is the probability of climate scenario j . io is the most probable ground-type.



1

2 Figure 2. An example of determining the probability distribution of organic layer thickness
3 for a land-cover type (C2, coniferous forest – medium density). a) Fitting the observed
4 relative cumulative frequency (the dash curve) with a modified logistic function (the bold
5 curve). The inset shows the scatter graph comparison and linear regression for the fitting. b)
6 The probability density (the bold curve), and the distribution of the ground-types and their
7 probabilities (the rectangle boxes).

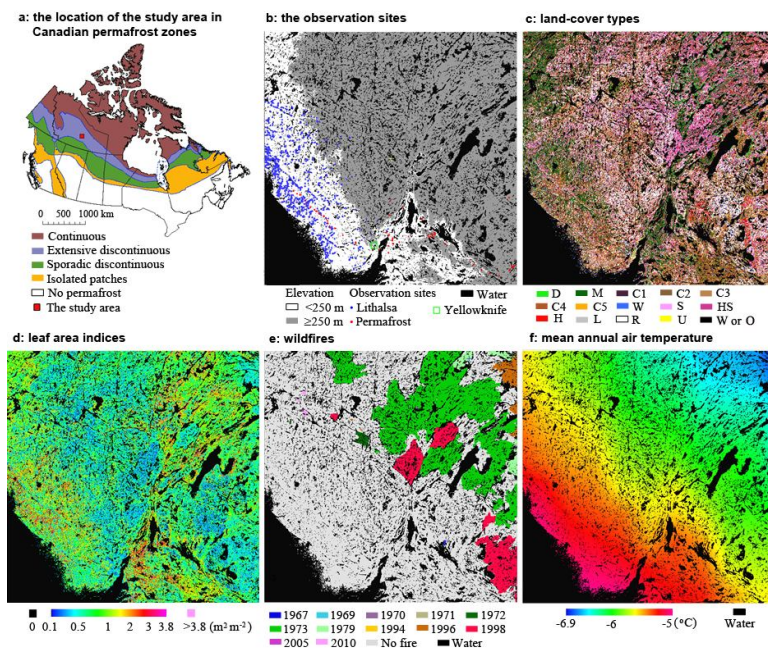


Figure 3. a) the location of the study area in Canadian permafrost zones (Heginbottom et al., 1995), b) the observation sites and the two regions divided based on elevation 205 m a.s.l., and the distributions of c) land-cover types, d) leaf area indices, e) wildfires, and f) thirty-year (1971-2000) mean air temperature in the study area.

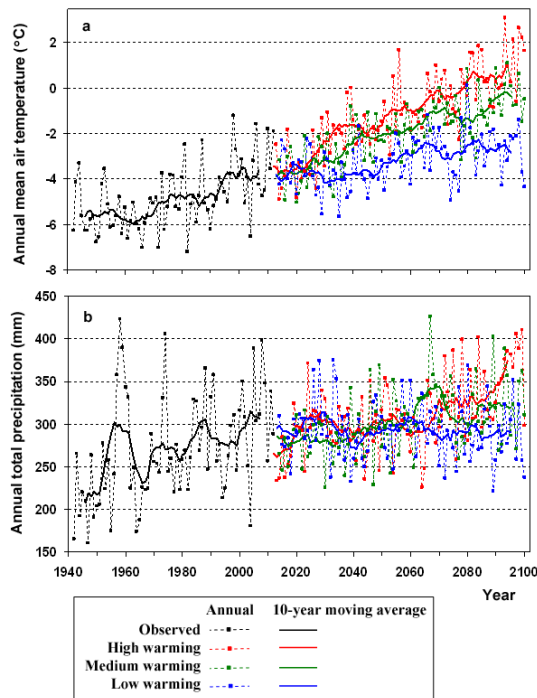


Figure 4. The historical climate trends and the selected three scenarios for the 21st century for a) annual mean temperature and b) annual total precipitation. The historical climate is observed at Yellowknife airport climate station. The low, medium and high warming scenarios were generated by CCCma (B1), CCCma (A1B) and MIROC (A1B), respectively. More details about the data and the climate models can be found at the World Data Center for Climate (<http://mud.dkrz.de/wdc-for-climate/>).

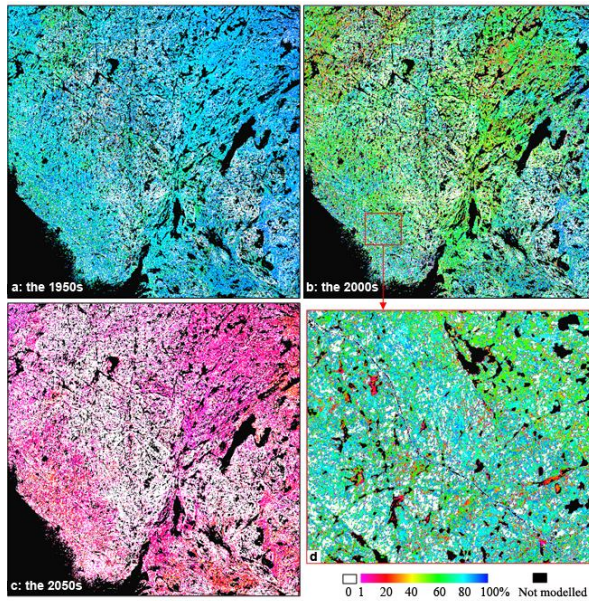


Figure 5. Modelled permafrost probability distributions in the 1950s, 2000s and 2050s (a, b, and c, respectively). Panel d shows an enlarged area in panel b.

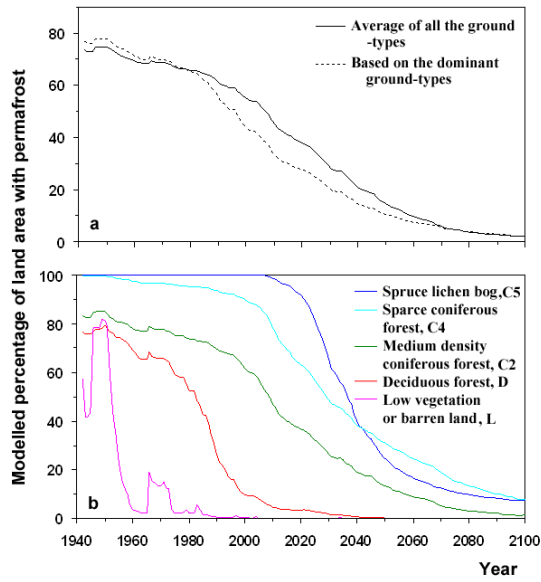


Figure 6. The modelled temporal changes of permafrost probability a) for the entire study area and b) for five selected land-cover types in this area.

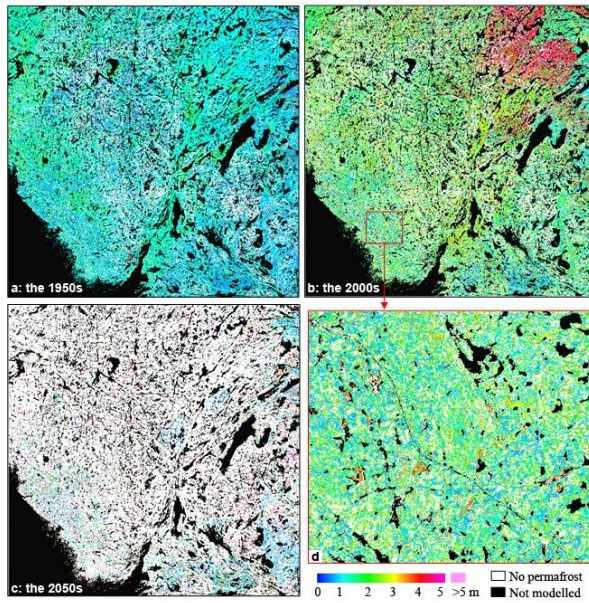


Figure 7. Modelled most likely active-layer thickness in the 1950s, 2000s and 2050s (a, b, and c, respectively). Panel d shows an enlarged area in panel b. This figure also shows the most likely distribution of permafrost (white color for non-permafrost areas, and the other colours (except black) for areas with permafrost).

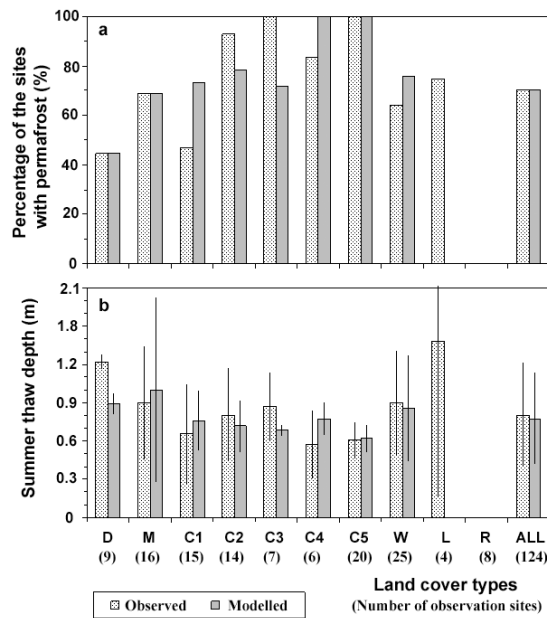
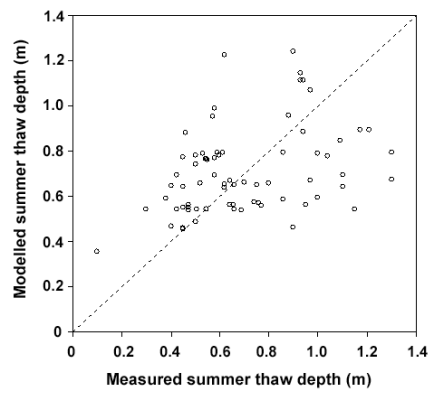
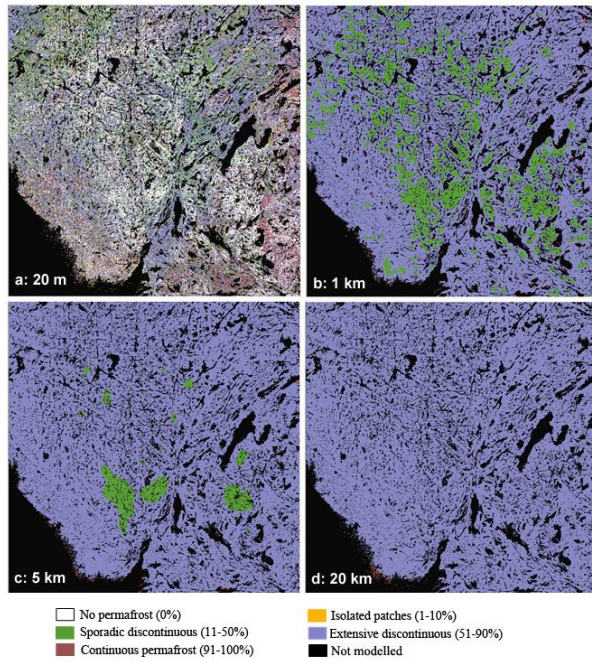


Figure 8. Comparisons of observed and modelled (a) percentage of the sites with permafrost and (b) the average and standard deviation of summer thaw depths for each land-cover type. The numbers in brackets below the x-axis are the numbers of observation sites. The average or the standard deviation of summer thaw depths were calculated based on the sites with permafrost (observed or modelled). The land-cover types S, SH and H were not shown because there were no field observations for these three types in the study area.



1

2 Figure 9. Comparison between the modelled and measured summer thaw depths. There are 71
 3 observation sites where both observation and the model show the existence of permafrost. The
 4 correlation coefficient is 0.365 ($n = 71$).
 5



1

2 Figure 10. The effects of spatial resolution (shown in the panels) on permafrost zonal
 3 distributions. These maps were produced by dividing permafrost probability in the 2000s (Fig.
 4 5b) into five zones and then re-sampled to different spatial resolutions.